Noname manuscript No.
(will be inserted by the editor)

On the modifications of near-inertial waves at fronts: Implications for energy transfer across scales

Leif N. Thomas

Received: date / Accepted: date

Abstract In the ocean, wind-generated kinetic energy (KE) manifests itself primarily in balanced currents and near-inertial waves. The dynamics of these flows is strongly constrained by the Earth's rotation, causing the KE in balanced currents to follow an inverse cascade but also preventing wave-wave interactions from fluxing energy in the near-inertial band to lower frequencies and higher vertical wavenumbers. How wind-generated KE is transferred to small-scale turbulence and dissipated is thus a non-trivial problem. This article presents a review of recent theoretical calculations and numerical simulations that demonstrate how some unusual modifications to internal wave physics by the lateral density gradients present at ocean fronts allow for strong interactions between balanced currents and near-inertial waves that ultimately result in energy loss for both types of motion.

Keywords fronts · internal waves · wave-mean flow interactions

1 Introduction

Winds blowing over the ocean generate currents with a range of frequencies. The bulk of the kinetic energy in these flows is contained in low frequencies, in mesoscale currents and eddies, all of which are strongly constrained by the Earth's rotation to follow the geostrophic balance. Winds also create near-inertial waves (NIWs), which are oscillatory, unbalanced motions with frequencies close to the inertial frequency $f = 2\Omega \sin \phi$ (Ω is the Earth's angular velocity and ϕ latitude). The dissimilar temporal scales of the balanced, mesoscale currents and the NIWs suggest that the two types of motion should not interact very effectively, and that the fast waves should simply pass

Leif N. Thomas
Department of Earth System Science
Stanford University, Stanford, California
E-mail: leift@stanford.edu

through the balanced flows without exchanging energy or momentum. While this is a fairly accurate characterization for weak mesoscale currents, this is not the case at ocean fronts where strong vertical vorticity and baroclinicity (i.e. lateral density gradients and their concomitant thermal wind shear) modify the properties of the NIWs and permit significant wave-mean flow interactions. Interactions caused by vertical vorticity have been studied extensively, both theoretically Mooers (1975),Kunze (1985), Young and Ben-Jelloul (1997). Lee and Niiler (1998), Klein et al (2003), Danioux et al (2008), Danioux et al (2015), Xie and Vanneste (2015) and observationally Kunze and Sanford (1984), Kunze (1986), D'Asaro (1995), van Meurs (1998), Elipot et al (2010), in contrast to those associated with baroclinicity. The objective of this article is to review recent work on how frontal density gradients facilitate wave-mean flow interactions and discuss their implications for the energetics of both the near-inertial wave field and balanced circulation in the ocean.

2 Modifications of near-inertial wave properties at fronts

The key to comprehending how fronts facilitate wave-mean flow interactions is to understand how baroclinicity modifies the propagation, frequency, and polarization relations of NIWs. For the latter two properties, the most insightful way to do this is to use parcel arguments and the principles of conservation of buoyancy and absolute momentum that govern the basic physics of inertia-gravity waves.

2.1 Parcel arguments and the minimum frequency of inertia-gravity waves

Buoyancy, $b = -g\rho/\rho_o$, (g is the acceleration due to gravity, ρ is the density, and ρ_o a reference density) is conserved when diabatic processes (caused by heating, cooling, or mixing of heat and salt, for example) are absent. Absolute momentum is an angular momentum-like quantity that is conserved in currents that are inviscid and that do not have spatial variations in the direction of their flow (which is a fairly good approximation at fronts). Take for example a current in the x-direction that satisfies these constraints. In this limit, both friction and pressure gradient forces in the along flow direction are zero, and the momentum equation in the x-direction can be written as

$$\frac{DM}{Dt} = 0 \tag{1}$$

where $M = u - fY$ is the absolute momentum, Y is the displacement of fluid parcels in the y-direction, and D/Dt is the material derivative. Thus $\Delta M \equiv \int (DM/Dt)dt = 0$, where Δ is the change following fluid parcels. Splitting the flow into two components, $u = u_g + u'$, one associated with the front, u_g, and the other with the wave, u', conservation of absolute momentum implies that

$$u' = -\Delta M_g \tag{2}$$

where $M_g \equiv u_g - fY$ is the absolute momentum of the background flow. The buoyancy can be decomposed in a similar fashion, $b = b_g + b'$, and if it is conserved the wave buoyancy anomaly is

$$b' = -\Delta b_g. \tag{3}$$

Wave buoyancy and velocity anomalies drive forces, the latter associated with the Coriolis force $-fu'$, that when restoring explain the oscillatory behavior of inertia-gravity waves.

For instance, in the textbook example with no background flow ($u_g = 0$) and a density field with flat isopycnals and stratification $N^2 = \partial b_g/\partial z$, small-amplitude vertical displacements, Z, generate a buoyancy anomaly and hence vertical acceleration $D^2Z/Dt^2 = b' = -N^2Z$, yielding oscillations at a frequency $\omega = N$. In this case, isosurfaces of the absolute momentum of the background flow, known as $M-$surfaces, are vertical (Fig. 1, upper left panel). Consequently, fluid parcel displacements in the $y-$direction cross $M-$surfaces and generate a velocity anomaly, Coriolis force, and lateral acceleration $D^2Y/Dt^2 = -fu' = -f^2Y$ but no buoyancy anomaly, and hence result in oscillations at a frequency $\omega = f$. For most oceanic conditions, $N > f$, and consequently inertia-gravity waves in the absence of a background flow span a range of frequencies between f and N as fluid parcel displacements move from being purely horizontal to purely vertical.

Fronts distort the geometry of isopycnals and M-surfaces, leading to profound modifications to the properties inertia-gravity waves. The baroclinicity of the front, which can be quantified with the thermal wind relation

$$S^2 \equiv -\frac{\partial b_g}{\partial y} = f\frac{\partial u_g}{\partial z}, \tag{4}$$

tilts both isopycnals and M-surfaces (Fig. 1, upper right panel). As the baroclinicity increases (keeping all other properties of the background flow constant), M-surfaces flatten while isopycnals steepen and the two surfaces angle towards one another. In this system, the inertia-gravity waves with the lowest frequency correspond to parcel displacements that are along-isopycnal (since they do not induce a buoyancy force), and result in oscillations caused by the Coriolis force, similar to the case without a background flow. However, the change in absolute momentum that the fluid parcels experience at a front, and hence the Coriolis force, is reduced because the along-isopycnal gradient in M is weakend by baroclinicity. The expression for the minimum frequency of inertia-gravity waves in a background flow reflects this physics

$$\omega_{min} = \sqrt{-f\nabla_\rho M_g} = f\sqrt{1 + Ro_g - 1/Ri_g}, \tag{5}$$

where $\nabla_\rho M$ is the along-isopycnal gradient in absolute momentum, which can also be written in terms of the gradient Rossby and Richardson numbers of the frontal, geostrophic flow:

$$Ro_g = \left(-\frac{\partial u_g}{\partial y}\right) \Big/ f \tag{6}$$

$$Ri_g = \frac{N^2 f^2}{S^4} \tag{7}$$

Whitt and Thomas (2013). The main message to take from (5) is that baroclinicity can lead to subinertial wave frequencies where $\omega_{min} < f$. In particular, for sufficiently low Richardson numbers, namely $Ri_g \to 1/(1+Ro_g)$, $\omega_{min} \to 0$ and the distinction in time scales between the waves and balanced currents is lost.

2.2 Polarization relations at the minimum frequency

For inertia-gravity waves at the minimum frequency, the polarization relation between the magnitudes of three components of the wave velocity is

$$(|u'_{min}|, |v'_{min}|, |w'_{min}|) = |v'_{min}| \left(\frac{\omega_{min}}{f}, 1, |s_\rho| \right), \tag{8}$$

where $s_\rho = S^2/N^2$ is the slope of isopycnals Whitt and Thomas (2013). Thus velocity hodographs of waves of minimum frequency do not trace perfect inertial circles but are instead ellipses with a major axis pointed in the cross-front direction (i.e. $|u'_{min}| < |v'_{min}|$) when $\omega_{min} < f$ (Fig. 1, lower panels). This follows from conservation of absolute momentum and the reduction of $|\nabla_\rho M|$ by baroclinicity. In addition, the hodographs are aligned with isopycnals which are tilted in the vertical, imparting a vertical velocity to the waves. These modifications allow the waves to flux momentum in the vertical and make the wave momentum fluxes anisotropic in the horizontal. This has important implications for the energetics of NIWs, as will be highlighted in sections 3 and 5.

2.3 Dispersion relation and wave propagation

While parcel arguments are useful for understanding the restoring forces for NIWs in fronts, they cannot be used to characterize wave propagation. Instead, a WKB-type analysis of the governing wave equation is the most straightforward approach to derive the waves' dispersion relation and group velocity.

Two-dimensional NIW are governed by the time-dependent, hydrostatic Eliassen-Sawyer equation

$$\left(\frac{\partial^2}{\partial t^2} + f_{eff}^2 \right) \frac{\partial^2 \psi'}{\partial z^2} + 2S^2 \frac{\partial^2 \psi'}{\partial y \partial z} + N^2 \frac{\partial^2 \psi'}{\partial y^2} = 0, \tag{9}$$

where $f_{eff} = f\sqrt{1+Ro_g}$ is the effective inertial frequency, and the wave velocity is related to the streamfunction in the usual way $v' = \partial\psi'/\partial z$, $w' = -\partial\psi'/\partial y$ Sawyer (1956), Eliassen (1962), Whitt and Thomas (2013). Assuming slow spatial variations in the background flow, plane wave solutions of the form

$\psi' \sim \exp[i(ly+mz-\omega t)]$ with wavevector (l, m) and frequency ω can be sought, yielding the dispersion relation

$$\omega^2 = f_{eff}^2 + 2S^2\gamma + N^2\gamma^2, \tag{10}$$

where $\gamma = l/m$. Similar relations were first derived by Mooers (1975) in the non-hydrostatic limit and by Kunze (1985) for fronts with weak vorticity and baroclinicity (i.e. with $Ro_g \ll 1$ and $Ri_g \gg 1$). The group velocity can be calculated from (10) as

$$\mathbf{c}_g \equiv \left(\frac{\partial\omega}{\partial l}, \frac{\partial\omega}{\partial m}\right) = \left(\frac{S^2 + N^2\gamma}{\omega m}\right)(1, -\gamma)\,. \tag{11}$$

It follows that the direction of energy propagation with respect to the horizontal, that is, the slope of wave characteristics, is

$$\frac{c_{g,z}}{c_{g,y}} = -\gamma = s_\rho \mp \sqrt{\frac{\omega^2 - \omega_{min}^2}{N^2}}. \tag{12}$$

For waves of a given frequency (excluding the minimum frequency) there are four possible directions of energy propagation, similar to inertia-gravity waves in the absence of a background flow. However, unlike the no-flow case, at a front the directions of propagation are symmetric about isopycnals not the horizontal (Fig. 2). Consequently for waves at the effective inertial frequency, $\omega = f_{eff}$, two characteristics slopes are possible $\gamma = 0$ and $-\gamma = 2s_\rho$, in contrast to the case of no front where only the $\gamma = 0$ characteristic and horizontal propagation is allowed. This leads to unusual rules for wave reflection off boundaries that can make NIWs undergo critical reflections during which energy from both the waves and mean flow is dissipated, as will be discussed in section 4.

2.4 Summary of modifications

Fronts modify the properties of NIWs in three important ways: first, by reducing the minimum frequency of inertia-gravity waves (5) they support waves with frequencies less than the effective inertial frequency f_{eff}; second, by adjusting the direction of energy propagation (12) they allow waves at the effective inertial frequency to transmit energy vertically as well as horizontally; and third, fronts permit vertical and anisotropic horizontal wave momentum fluxes as a consequence of the polarization relation (8). These modifications are important because they are responsible for phenomena that could help close the energy budgets of both the NIW field and balanced circulation, as will be described in the next three sections.

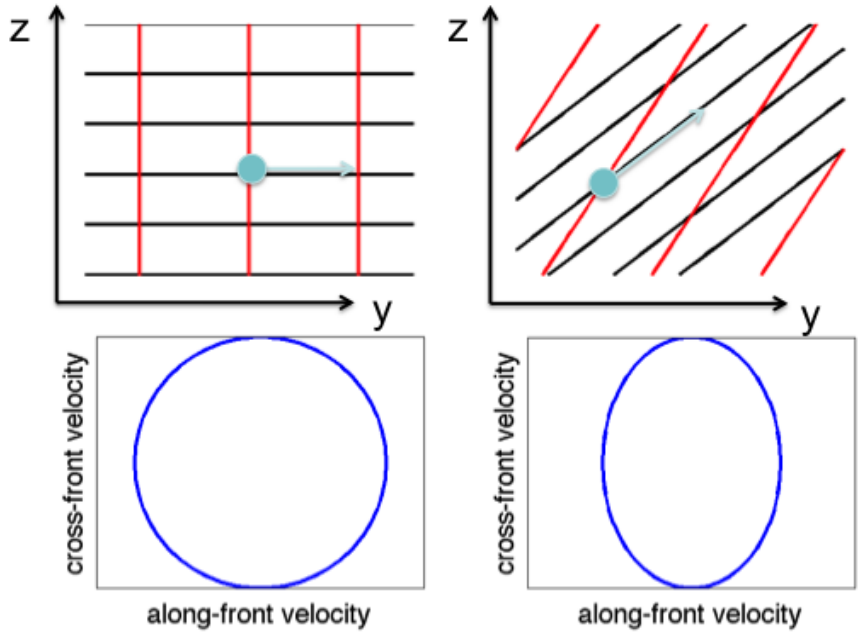

Fig. 1 Upper panels: isopycnals (black) and $M-$surfaces (red) for no background flow (left) and at a front (right), where thermal wind shear and horizontal density gradients tilt the two surfaces towards one another and reduce the along-isopycnal gradient in absolute momentum. Consequently, at fronts along-isopycnal displacements of fluid parcels (blue arrows), which lead to inertia-gravity waves with the minimum frequency, result in a reduced along-front wave velocity, u', Coriolis force, and frequency. In addition, hodographs of the wave velocity (bottom panels) shift from inertial circles when there is no background flow (left) to ellipses with stronger flow in the cross-front direction at a front (right).

3 Parameteric subharmonic instability at fronts

In the upper ocean, the majority of the kinetic energy (KE) in the internal wave spectrum is found near the inertial frequency Ferrari and Wunsch (2009). How NIWs lose their KE is not well understood although shear instabilities, wave absorption at critical layers, and energy transfer via wave-wave interactions have been proposed as possible damping mechanisms Alford and Gregg (2001), Kunze et al (1995), Müller et al (1986). One wave-wave interaction, parametric subharmonic instability (PSI), that is normally eliminated from this list is characterized by a transfer of energy from a wave of a given frequency to its subharmonic at half its frequency. Since NIWs have the lowest frequencies of all inertia-gravity waves according to classical internal wave theory, they cannot lose energy via PSI. However, this reasoning no longer holds at fronts because baroclinicity permits inertia-gravity waves with subinertial frequencies, e.g. (5). Indeed, Thomas and Taylor (2014) demonstrated using a stability analysis and numerical simulations that inertial waves in fronts can be damped by PSI

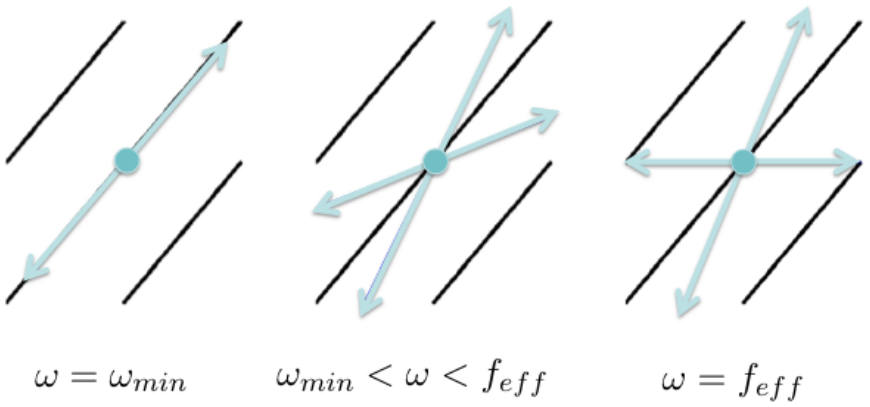

Fig. 2 The directions of energy propagation for NIWs, i.e. the ray paths, (blue arrows) are parallel to isopycnals (black lines) at the minimum frequency ω_{min} (left) and progressively move away from the isopycnal slope as the frequency is increased. This is very different from NIWs in the absence of background currents, which propagate horizontally at the minimum frequency. At a front, horizontal propagation only occurs for waves at the effective inertial frequency, $\omega = f_{eff}$, yet these waves can also propagate vertically on a steep characteristic with twice the isopycnal slope.

under certain conditions. The key findings from this work are summarized in this section.

Thomas and Taylor (2014) considered a vertically-sheared inertial oscillation superimposed on a simple front with uniform gradients (Fig. 3). The frontal flow had no vertical vorticity and hence the inertial motion oscillated at a frequency $f_{eff} = f$. Therefore the condition for PSI to develop at the front is $\omega_{min} \leq f/2$, which using (5) translates to a critical Richardson number of $Ri_g = 4/3$. Thomas and Taylor (2014) tested this prediction using a stability analysis in which the basic state was perturbed with a two-dimensional (invariant in the along-front direction) plane wave corresponding to an inertia-gravity wave of minimum frequency, i.e. with flow that is aligned with isopcynals (Fig. 3, black arrows). Time series of the cross-front velocity of the perturbations for three values of the Richardson number $Ri_g = 7/6, 4/3$, and $3/2$ illustrate the expected increase in frequency of the perturbation, but also growth for $Ri_g = 4/3$ when $\omega_{min} = f/2$ and PSI is active (Fig. 4, middle panel). This result is for weak inertial shear. The stability analysis revealed that the instability criteria is also a function of the strength of the inertial shear relative to the thermal wind shear. When it is weak, PSI occurs near $Ri_g = 4/3$ as illustrated above, but as the two shears become comparable, PSI can develop for a range of values of Ri_g centered about 4/3 since the inertial shear affects the properties of the waves Thomas and Taylor (2014).

PSI gains energy by extracting KE from the inertial oscillation at a rate given by the ageostrophic shear production

$$AGSP = -v'w'\frac{\partial \overline{v}}{\partial z} \tag{13}$$

where $\overline{v}$ is the cross-front velocity of the inertial motion and v', w' are the velocity components of the perturbation. Since the perturbation is a wave of minimum frequency, its velocity is along-isopycnal and v' and w' are correlated following the polarization relation (8). This results in a vertical wave momentum flux that can lead to a net extraction of KE from the inertial oscillation with $AGSP > 0$ when the flux is phased correctly with the inertial shear (Fig. 4, bottom panel). This phasing is achieved when $\omega_{min} = f/2$ (namely when the perturbation wave is a subharmonic of the inertial motion, hence the PSI) and when the times of minimum inertial shear and maximum $|v'|$ coincide (c.f. Fig. 4, top and middle panels, black lines)[1].

Thus, at fronts, PSI can remove KE from inertial motions, but what is the ultimate fate of this energy? Nonlinear, non-hydrostatic, high-resolution numerical simulations were used by Thomas and Taylor (2014) to address this question and test the stability analysis. The simulations were configured with a front and inertial oscillation similar to that used in the stability analysis, however the perturbations were initialized with random noise rather than a plane wave. Out of the noise, an unstable mode with flow parallel to isopycnals grows under the conditions for PSI to develop predicted by the stability analysis (Fig. 5, left panel). As it grows in amplitude, the unstable mode develops secondary shear instabilities, creating Kelvin-Helmholtz billows in the regions of strong shear where the Richardson number of the total flow drops below a quarter. The unstable mode extracts KE from the inertial shear via the AGSP, consistent with the stability analysis. However, the amount of KE contained in the perturbations saturates at a value much less than the total KE removed from the inertial motion (Fig. 5, right panel). The remaining KE is not stored in the unstable mode, but is instead either lost through viscous dissipation or increases the potential energy of the system through mixing density by the small-scale shear instabilities. It is important to realize that these shear instabilities would not form in the absence of the PSI because the minimum Richardson number of the combined geostrophic and inertial motions is above the criterion for Kelvin-Helmholtz instability. By enhancing the vertical shear, the growth of the PSI lowers the Richardson number to subcritical values, thereby opening a pathway to turbulence where KE in inertial motions is transferred to small scales and lost.

4 Critical reflection of near-inertial waves at fronts

Apart from wave-wave interactions such as PSI, inertia-gravity waves can lose energy during reflections off boundaries. This is especially true if they experience critical reflection, when the direction of energy propagation of the reflected wave runs parallel to the boundary Ivey and Nokes (1989). Accord-

[1] This is true for a front with upward sloping isopycnals where v' and w' are positively correlated as shown in Fig. 3, and as used in the stability analysis plotted in Fig. 4. When isopycnals slope downward, the times of *maximum* inertial shear and maximum $|v'|$ must coincide for PSI to develop since v' and w' are anti-correlated in that case.

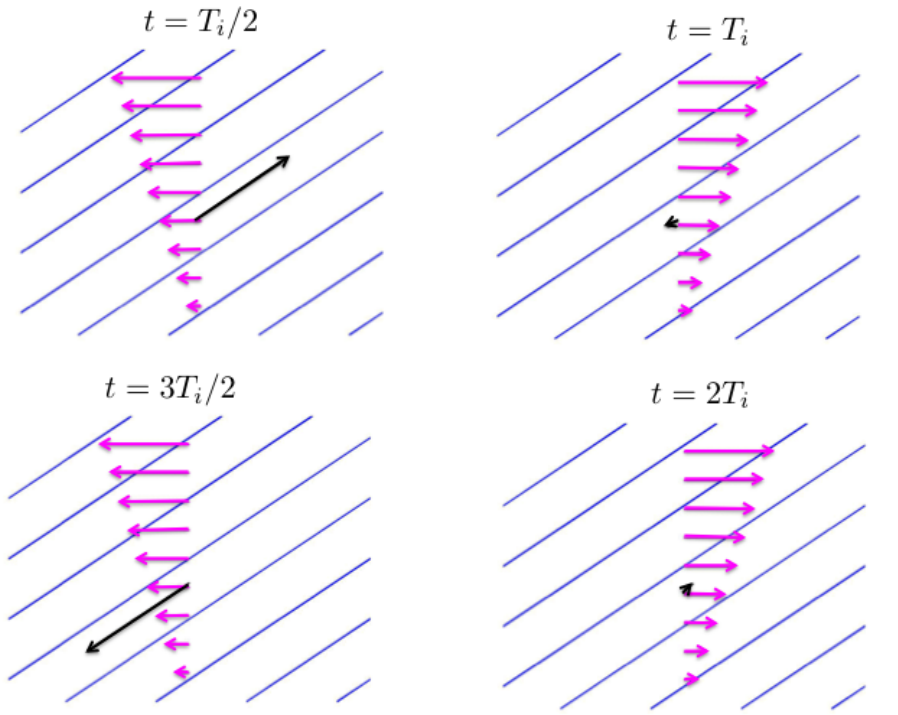

Fig. 3 Schematic of the basic state of the stability analysis used to study a parametric subharmonic instability that extracts kinetic energy from inertial motions at fronts. A vertically-sheared inertial oscillation (velocity vectors in magenta) at a front (isopcynals in blue) is perturbed by a flow that is purely isopycnal (velocity vector in black). Four snapshots are shown, at $1/2, 1, 3/2$, and 2 inertial periods, T_i, and for a front with $Ri_g = 4/3$.

ing to classical internal wave theory ($u_g = 0$), inertial waves with $\omega = f_{eff} \equiv f$ cannot experience critical reflection because they only propagate horizontally. At fronts, however, this conclusion does not hold because inertial waves can propagate in the vertical as well as in the horizontal (e.g. Fig. 2). Using analytical theory and numerical simulations, Grisouard and Thomas (2015) and Grisouard and Thomas (2016) demonstrated that inertial waves can indeed experience critical reflection as a consequence of this physics. A summary of this work is presented in this section.

If an inertial wave is propagating vertically in a front along the tilted ray path shown in the righthand panel of Fig. 2, when it hits a boundary it must reflect along the horizontal characteristic with $\gamma = 0$. Consequently, if the boundary is flat, a beam of inertial wave energy will be compressed into an infinitesimally thin area upon reflection and the wave must amplify to conserve its energy. This is the condition for critical reflection and it can occur at fronts off the nominally-flat sea surface (Fig. 6). Grisouard and Thomas (2015) tested this idea using linear and nonlinear numerical simulations. The simulations were forced by a wave maker at depth that was designed to generate upward

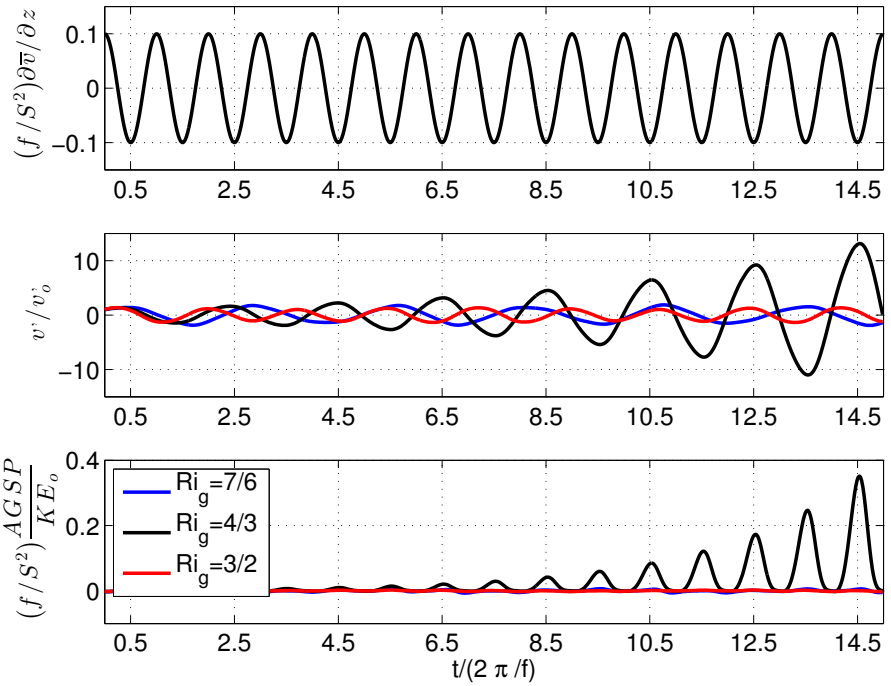

Fig. 4 Results from the stability analysis for a basic state similar to that shown in Fig. 3, but with three different Richardson numbers of the frontal flow $Ri_g = 7/6, 4/3, 3/2$ (blue, black, and red lines, respectively) yet the same inertial shear (top panel, normalized by the thermal wind shear S^2/f). Time series of the perturbation cross-front velocity (middle panel, normalized by its initial value) and the ageostrophic shear production (13) (bottom panel, normalized by $(S^2/f)KE_o$, where KE_o is the initial kinetic energy of the perturbation). Time is expressed in units of inertial periods.

propagating waves on the steep characteristic of (12). In the linear simulations, inertial waves on the steep characteristic are amplified upon reflection, but the amplification is limited by friction in a thin viscous boundary layer that develops near the surface (Fig. 7). In the nonlinear simulations bores and higher harmonics form via wave-wave interactions, resulting in a thicker layer over which the effects of critical reflection are felt Grisouard and Thomas (2015), but the basic energetics of the phenomenon are qualitatively similar.

The energy fluxed upwards by the wave maker,

$$\text{Incoming Flux} = \int p'w'dy, \tag{14}$$

(where p' is the wave pressure perturbation, and the integral is made over the width of the domain) is dissipated in the boundary layer during critical reflection. However, the total dissipation of wave energy (both kinetic and potential),

$$\text{Dissipation} = \nu \int\int \left(\mathbf{u}' \cdot \frac{\partial^2 \mathbf{u}'}{\partial z^2} + \frac{b'}{N^2} \frac{\partial^2 b'}{\partial z^2} \right) dydz, \tag{15}$$

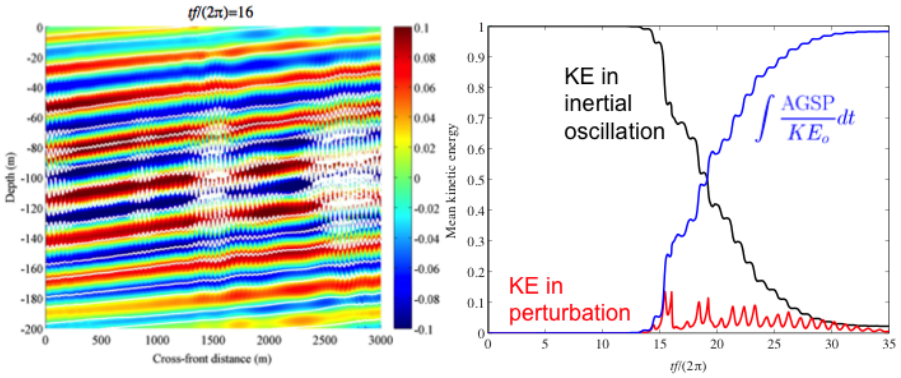

Fig. 5 Left: The cross-front velocity (color shading, in units of m s^{-1}) and isopycnals (white contours) at 16 inertial periods into a numerical simulation of a front with and inertial shear, similar the set up shown in Fig. 3, however initialized with perturbations taking the form of random noise. Over time perturbations with flow parallel to isopycnals grow out of the noise and develop Kelvin-Helmholtz billows that are evident in the fine-scale structures in density. Right: Time series from the simulation of the kinetic energy in the inertial shear (black) and the perturbations (red), and the kinetic energy removed from the inertial shear by the perturbations $\int AGSPdt$. Variables are normalized by the initial kinetic energy in the inertial oscillation and time by an inertial period.

(where ν is the constant viscosity and diffusivity used in the simulations and the integral is made over a control volume that spans the width and upper 15 meters of the domain) exceeds the incoming flux for waves near critical reflection with $\omega \approx f$ (Fig. 8, upper panel) Grisouard and Thomas (2016). Clearly there must be an additional source of wave energy besides the wave maker to explain this excess dissipation. This extra energy originates from the front and is liberated by the waves at a rate

$$\text{Energy exchange with Front} = \int\int \left(-u'w' \frac{S^2}{f} + v'b' \frac{S^2}{N^2} \right) dydz, \qquad (16)$$

where the control volume is the same as that used in (15) (Fig. 8, bottom panel). Near critical reflection, the waves preferentially remove the front's potential energy over its kinetic energy via the second term in (16), indicating that they act to mix the frontal lateral density gradient.

The rate of energy removed from the front depends on both the wave frequency and the strength of the fronts, as measured by the Richardson number (Fig. 8, bottom panel). The energy exchange with the front involves correlations between the wave velocity components and its buoyancy anomaly. Friction enhances these correlations, consequently they are largest at near-inertial frequencies where viscous effects are most prominent due to the compression of the waves' vertical scale near critical reflection Grisouard and Thomas (2016). The peak energy exchange at near-inertial frequencies decreases with increasing Richardson number, which is to be expected since the front is weaker. In addition, as Ri_g increases, the slope of isopycnals and hence characteristics of

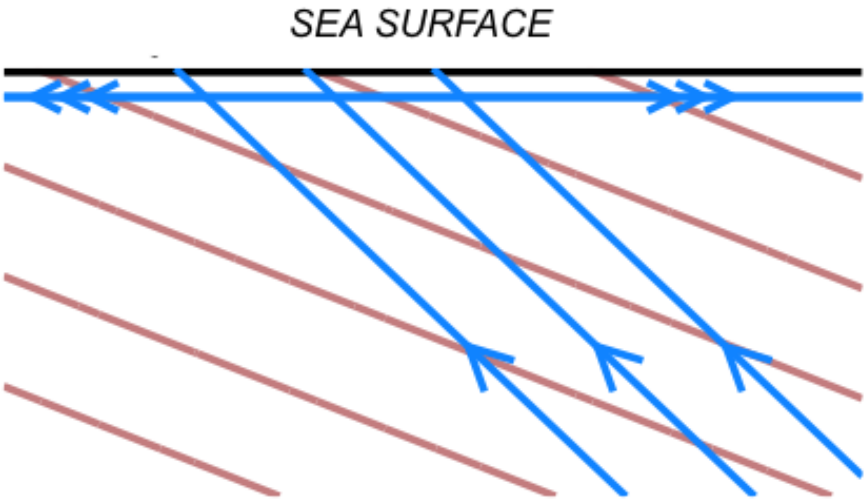

Fig. 6 At a front (isopycnals in brown) a beam of energy associated with a vertically propagating inertial wave with $\omega = f_{eff}$ (blue, upward sloping lines), will be compressed into an infinitesimally-thin area when the wave reflects off the sea surface. Under these conditions the wave experiences critical reflection and amplifies.

vertically-propagating inertial waves, c.f. (12), is reduced. Consequently, the amplification of the waves by the compression of ray tubes during critical reflection (c.f. Fig. 6) is less intense. Since the waves in the boundary layer are weaker, the energy exchange with the front is reduced. For the strongest fronts (with Richardson numbers near one), however, the rate of energy exchange is comparable to the incoming energy flux of the waves, suggesting that critical reflection of inertial waves at fronts acts as a damping mechanism for the balanced circulation that depends externally on the processes that generate the inertial waves either locally or non-locally, such as the tides or the winds.

5 Near-inertial waves in fronts undergoing frontogenesis

The wave-mean flow interactions that have been described thus far involve fronts with lateral density gradients that do not change with time. In the ocean, however, the strength of fronts is rarely stationary, but evolves in response to frontogenetic and frontolytic processes. Strain imposed by the flow of mesoscale eddies is particularly effective at modifying lateral density gradients. When the strain is frontogenetic, it leads to a rapid intensification of the thermal wind shear and a decrease in the gradient Richardson number of the frontal, geostrophic flow (7). As a result, NIWs caught up in a front undergoing frontogenesis, should experience considerable modifications to their dispersion and polarization relations (e.g. section 2), that could foster wave-mean flow

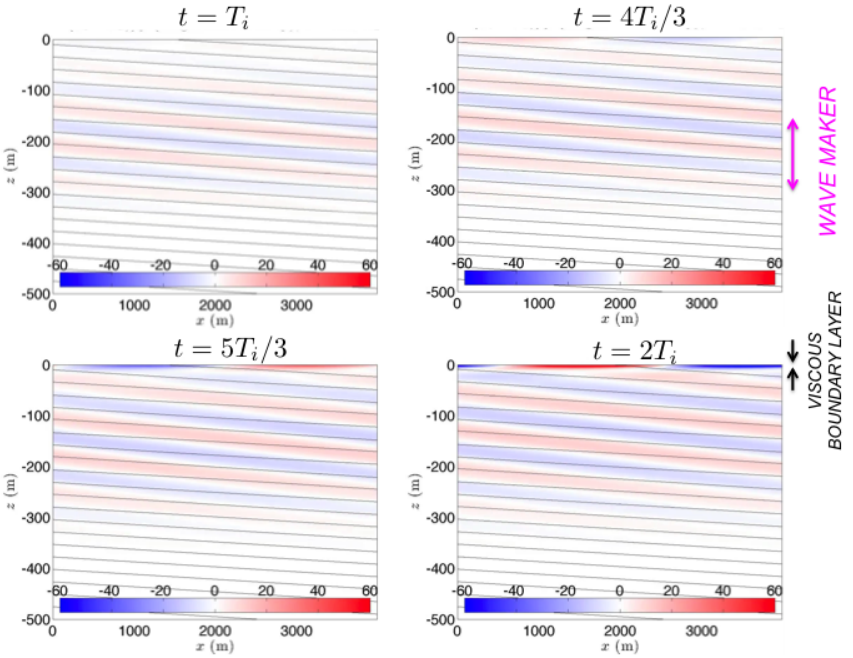

Fig. 7 Snapshots of an inertial wave (i.e. with frequency $\omega = f$) at $1, 4/3, 5/3$, and 2 inertial periods in a front with isopycnals in black from a linear numerical simulation. The wave is forced by a wave maker at the depth indicated by the magenta arrow to the right that generates an upward propagating wave packet. As the waves hit the surface, they experience a critical reflection and generate a thin viscous boundary layer.

interactions. This idea was explored in the theory of Thomas (2012), which will be summarized here and illustrated with a numerical simulation.

As in the front-NIW interactions studies described in the previous sections, Thomas (2012) used the simple "frontal-zone" configuration with spatially-uniform gradients in the density and flow fields (e.g. Fig. 9). In contrast to those studies, the frontal zone is forced by an additional flow $(u_e, v_e) = (\alpha x, -\alpha y)$ with a constant strain, α, that is frontogenetic. This flow is balanced and is meant to represent a mesoscale eddy-driven strain field. The strain throws the front out of the thermal wind balance, and drives an ageostrophic circulation to restore geostrophy. For this simple configuration, the ageostrophic flow is in the cross-front direction, is sheared in the vertical, and drives restratification (Fig. 9, magenta arrows). In spite of the strengthening stratification, however, Ri_g decreases in time because of the exponentially-growing thermal wind shear (Fig. 10, lower panel). The Richardson number of the frontal flow eventually asymptotes to one, reflecting the tendency for frontogenesis to

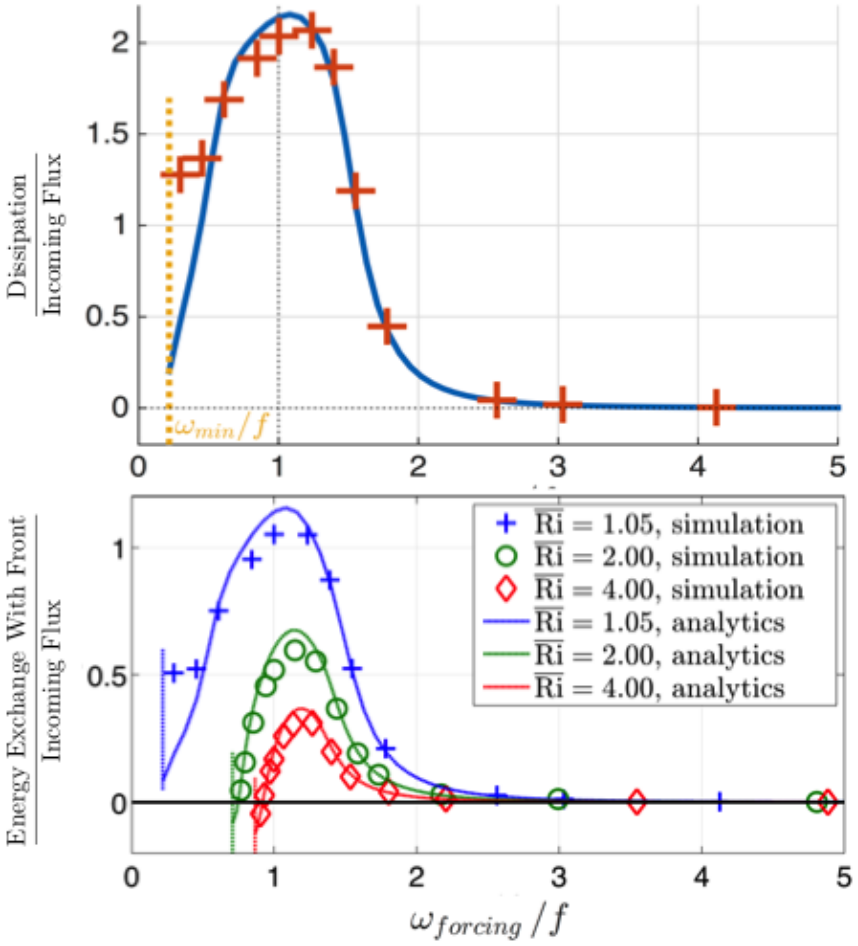

Fig. 8 Top panel: the dissipation of energy integrated over a control volume that spans the upper 15 meters of the domain, (15), normalized by the energy flux of the upward propagating wave, (14), as a function of the forcing frequency of the wave generator, $\omega_{forcing}$. The Richardson number of the front is $Ri_g = 1.05$, with a minimum wave frequency indicated by the vertical, yellow dashed line. Bottom panel: the rate of energy exchange with the front integrated over a control volume that spans the upper 15 meters of the domain, (16), normalized by the energy flux of the upward propagating wave, (14), as a function of the forcing frequency of the wave generator, for three different frontal flows with Richardson numbers $Ri_g = 1.05, 2$, and 4. Solid lines (markers) indicate results from the theory (linear numerical simulations).

cause surfaces of constant density and absolute momentum to run parallel to one another over time (Fig. 10, top panels)[2].

[2] Note that for this simple frontal zone without vertical vorticity, the slope of $M-$surfaces is $s_M = f^2/S^2 = Ri_g s_\rho$. Hence as $Ri_g \to 1$, s_M approaches the isopycnal slope s_ρ.

To this background flow, Thomas (2012) added a two-dimensional near-inertial wave (i.e. invariant in the along-front direction) with streamlines that run parallel to isopycnals (Fig. 9, blue lines) and solved for the evolution of its velocity. In the absence of frontogenetic forcing, this wave would correspond to the inertial-gravity wave of minimum frequency described in section 2. However, because of the time-dependent nature of the background flow and the presence of ageostrophic shear, the wave is not a simple periodic motion with stationary frequency and amplitude. For early times when Ri_g is large, the amplitude and frequency are relatively constant and the two horizontal components of the velocity oscillate in quadrature as a near-inertial motion (Fig. 11, top panel). However, as the front strengthens and Ri_g asymptotes to 1, both the wave's frequency and amplitude decrease. The reduction in amplitude is more pronounced for the along-front versus cross-front component of the velocity (u' and v', respectively), making the velocity hodograph shift from an inertial circle early in the record to a more rectilinear flow in the cross-front direction over time (Fig. 11, lower left panel). This behavior is consistent with the effect that lateral density gradients have on the polarization relation of NIWs described in section 2, and can be understood in terms of conservation of absolute momentum. As the front strengthens and isopycnals and M-surfaces align, along-isopycnal wave parcel displacements cross fewer and fewer M-surfaces over time, therefore reducing the amplitude of the along-front velocity perturbation u' required to conserve absolute momentum. As u' weakens, so too does the Coriolis force that provides the restoring force for the oscillation, and consequently the periods between velocity minima and maxima expand as frontogenesis progresses (Fig. 11, top panel).

The wave is ultimately damped, however not by friction as the theory is inviscid, but by transferring kinetic energy to the background flow. The wave can exchange energy with all three elements of the background flow: the thermal wind shear, the balanced eddy strain field, and the cross-front ageostrophic shear at rates $GSP = -u'w'(S^2/f)$,

$$DSP = -u'^2\frac{\partial u_e}{\partial x} - v'^2\frac{\partial v_e}{\partial y} = \alpha(v'^2 - u'^2) \tag{17}$$

and $AGSP$ (e.g. (13), where $\overline{v}$ in this context represents the ageostrophic flow driven by frontogenesis), respectively. These three shear production terms can be non-zero only if the waves induce a vertical flux of momentum, or if their horizontal momentum flux is anisotropic. Fronts allow this to happen by modifying the wave polarization relations, as discussed in section 2 and as manifest in the solution shown in Fig. 11. Time integrals of the three shear production terms reveal that the waves lose KE to the ageostrophic shear via $AGSP$ (Fig. 12, red line). Surprisingly, however, the waves lose twice the amount of KE that they started with through this mechanism. The additional KE that can account for this discrepancy originates from the strain field via DSP (Fig. 12, black line), which only becomes a major player in the wave energetics when the wave velocity becomes rectilinear and $|v'|$ exceeds $|u'|$ and (17) becomes positive. The dominance of the cross-front wave velocity at this time drives

a momentum flux v'^2 that is down the gradient of v_e (Fig. 11, lower right panel). In this way, the waves act like a viscosity for the balanced eddy-driven strain field. The KE transferred from the deformation field is ultimately lost to the unbalanced ageostrophic circulation through shear production, hence the waves play a catalytic role in loss of balance. The energy exchange is quite rapid, occurring over a few inertial periods, and scales with the KE initially contained in the waves. Given the large amount of KE in NIWs and the ubiquitous combination of eddy strain and fronts in the ocean, this mechanism could play a significant role in the removal of KE from both the internal wave and mesoscale eddy fields.

In spite of the many simplifying assumptions for the flow configuration used in the theory of Thomas (2012) (e.g. the frontal gradients and strain considered were spatially uniform and the flow was unbounded) the predictions of the theory are qualitatively borne out in numerical experiments of NIWs in strained fronts with more realistic flow fields. One such numerical experiment will be presented here, while a more thorough examination is described in Thomas (2016). The numerical simulation is configured with a front that is aligned in the x-direction, with initially uniform gradients, and in a periodic channel with walls on the northern and southern boundaries of the domain (Fig. 13, left panel). The front is in geostrophic balance, and an array of barotropic eddies is added to the flow to generate strain. The strain is frontogenetic near $y = 37.5$ km, $x = 18.75$ km and frontolytic near $y = 37.5$ km, $x = 56.25$ km (Fig. 13). To this flow a NIW is added that takes the shape of a plane wave modulated in the north-south and vertical directions to form a beam (Fig. 14, upper panels). The response of the wave to frontogenetic versus frontolytic strain is markedly different (c.f. Fig. 14 and Fig. 15 left and right panels). In regions of frontolysis, the horizontal wavenumber of the wave decreases as isopycnals flatten and the front weakens. The wave essentially retains its inertial character throughout the simulation as reflected in its velocity hodograph that traces inertial circles (Fig. 15 left panel). In contrast, in regions of frontogenesis the properties of the wave change dramatically: the horizontal wavenumber increases, the amplitude decreases, and the velocity becomes more rectilinear in the cross-front direction with time (Fig. 14 and Fig. 15 left panels). The modifications to the NIW in the front undergoing frontogenesis is therefore qualitatively consistent with the theory (e.g. Fig. 11).

A more quantitative comparison to the theory can be made by calculating the transfer of kinetic energy from the balanced strain field to the wave, $\int DSPdt'$. In the region of frontogenesis an amount of kinetic energy is removed from the strain field that is smaller than, yet comparable, to the initial KE in the NIW by the end of the experiment (c.f. Fig. 16 left and right panels). This behavior is consistent with the theory (e.g. Fig. 12, black line), but unlike the theory, the energy exchange occurs in a narrow zone delineated by the finite width of the front.

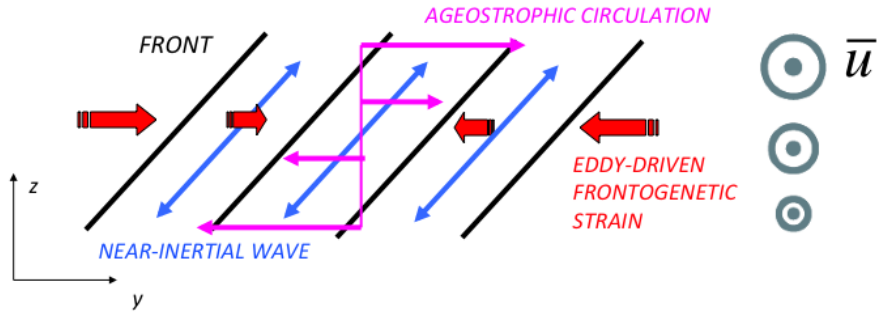

Fig. 9 Flow configuration used in the theory to study NIWs in a front undergoing frontogenesis. A front (with isopycnals in black) is forced by a frontogenetic strain field (red arrows). Both the density gradient and strain are spatially-uniform and the domain is unbounded. To maintain the thermal-wind balance in the presence of strain, a vertically-sheared ageostrophic secondary circulation (with velocity vectors in magenta) is induced. A two-dimensional (i.e. invariant in the x-direction) near-inertial wave (with phase lines shown in blue) is added to the flow.

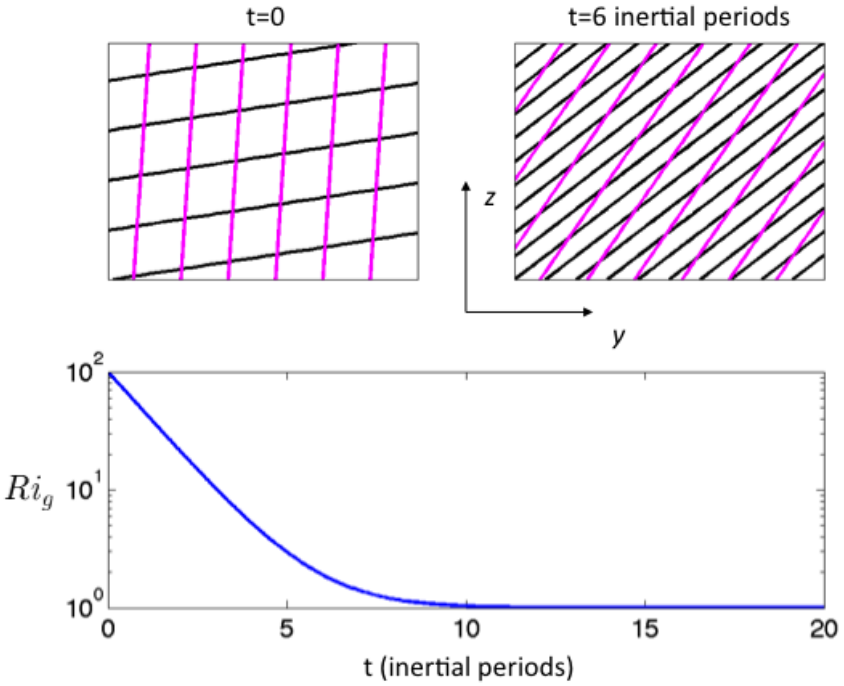

Fig. 10 Surfaces of constant absolute momentum M_g, (magenta) and isopycnals (black) of the frontal zone schematized in Fig. 9 at the onset of frontogenesis, top left, and six inertial periods later, top right, for a front forced by a strain of strength $\alpha = 0.0625f$. The gradient Richardson number of the frontal flow, Ri_g, is plotted as a function of time in the bottom panel and in this particular example is initially equal to 100 but asymptotes to one under frontogenesis.

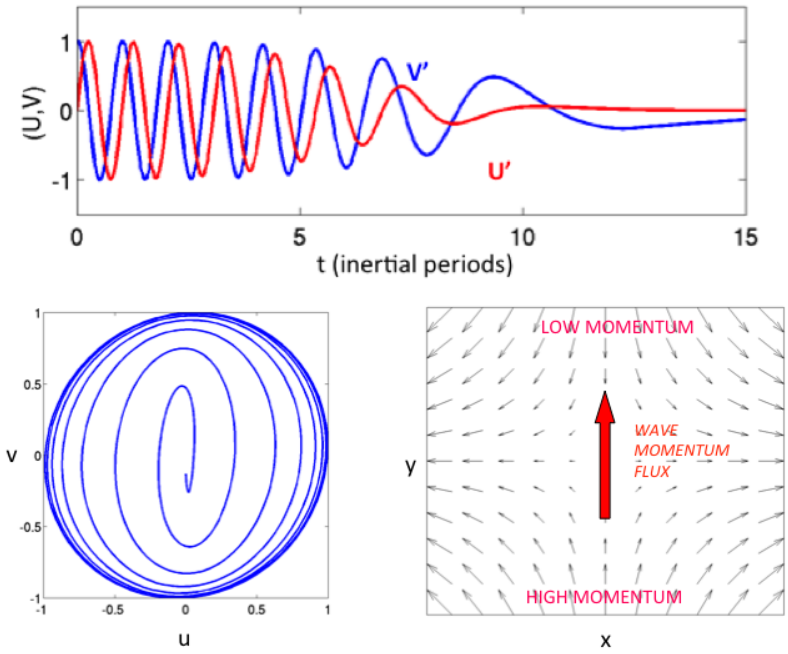

Fig. 11 Top panel: Change in the along-front, u' (red), and cross-front, v' (blue), components of the velocity of a near-inertial wave in the background flow undergoing frontogenesis shown in Fig. 10. Bottom left panel: a hodograph of the velocities in the top panel reveals how a near-inertial wave in a front undergoing frontogenesis experiences a change in polarization relation, transitioning from being circularly polarized to rectilinear in the cross-front, y-direction. In the process, the wave induces a momentum flux that is down the gradient in momentum associated with the eddy-driven strain field whose velocity $(\alpha x, -\alpha y)$ is shown in plan view in the bottom right.

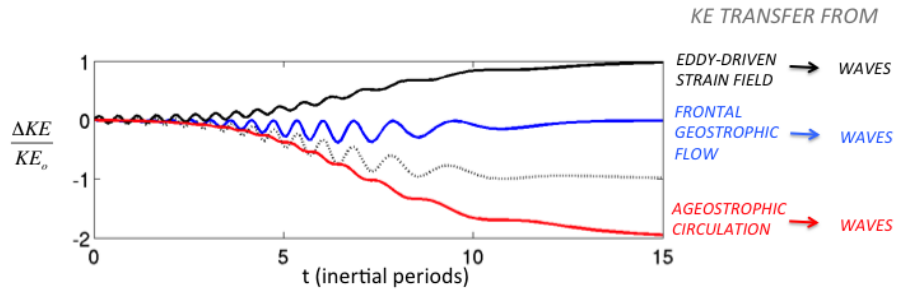

Fig. 12 The transfer of KE to the near-inertial wave shown in Figure 11 from the eddy-driven strain field, $\int_0^t DSP/KE_o dt'$ (black), the frontal geostrophic flow, $\int_0^t GSP/KE_o dt'$ (blue), and the ageostrophic circulation, $\int_0^t AGSP/KE_o dt'$ (red). The dotted black line is the sum of all three terms and represents the net change in KE of the wave. All quantities are normalized by the initial KE of the wave, KE_o.

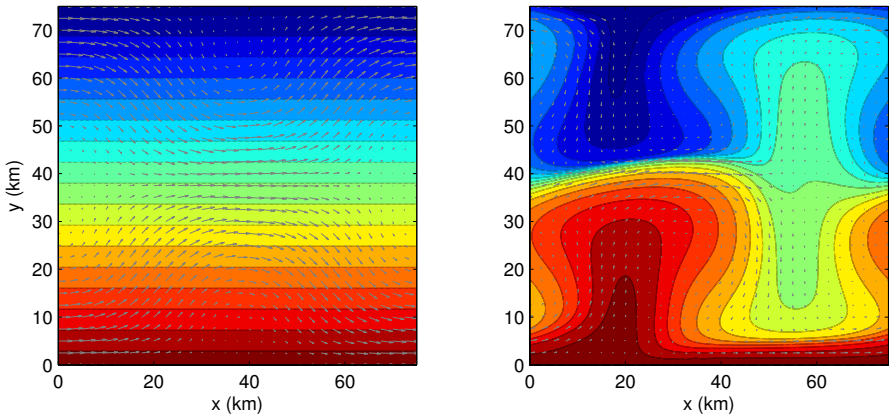

Fig. 13 Plan view of the surface buoyancy and velocity fields at $t = 0$ (left) and 7.1 inertial periods (right) from the numerical simulation used to study NIWs in a front undergoing frontogenesis. The eddy field that drives frontogenesis (frontolysis) near $x = 18.75$ km, $y = 37.75$ km ($x = 56.25$ km, $y = 37.75$ km) has an initial maximum strain rate of $0.045f$.

6 Conclusions

Winds are one of the main sources of KE for the ocean and generate NIWs and balanced currents. How the KE contained in these motions is transferred to small scales and dissipated is not well understood. Wave-mean flow interactions have been invoked as a mechanism that could facilitate this process. Here, it is shown that ocean fronts, which are a ubiquitous feature of the upper-ocean, provide conditions conducive for irreversible energy exchanges between NIWs, balanced motions, and small-scale turbulence by modifying the properties of the waves in rather unusual ways.

In fronts, inertia-gravity waves are permitted to have subinertial frequencies, more accurately, frequencies that are less than the effective inertial frequency $f_{eff} = f\sqrt{1 + Ro_g}$. Consequently, at fronts NIWs can be susceptible to a parametric subharmonic instability that transfers KE from the waves to subinertial motions with smaller vertical scales; subsequent development of secondary instabilities irreversibly convert the NIW KE to potential energy and heat through mixing and viscous dissipation. This PSI develops in stratified frontal flows with Richardson numbers just above one, well above the condition for Kelvin-Helmholtz instability. Such conditions are likely to be found at the base of the surface mixed layer in the ocean. It is precisely in this region where inertial shears, the source of energy for the PSI, are observed to be strongest and where much of the near-surface dissipation of inertial motions is thought to occur Plueddemann and Farrar (2006). Could PSI facilitate this dissipation? To investigate this possibility more fully, the effects on the instability of vertically-varying stratification and shear should be studied.

The four directions that energy in an inertia-gravity wave can propagate are symmetric about the isopycnal slope, not the horizontal, which at a front can

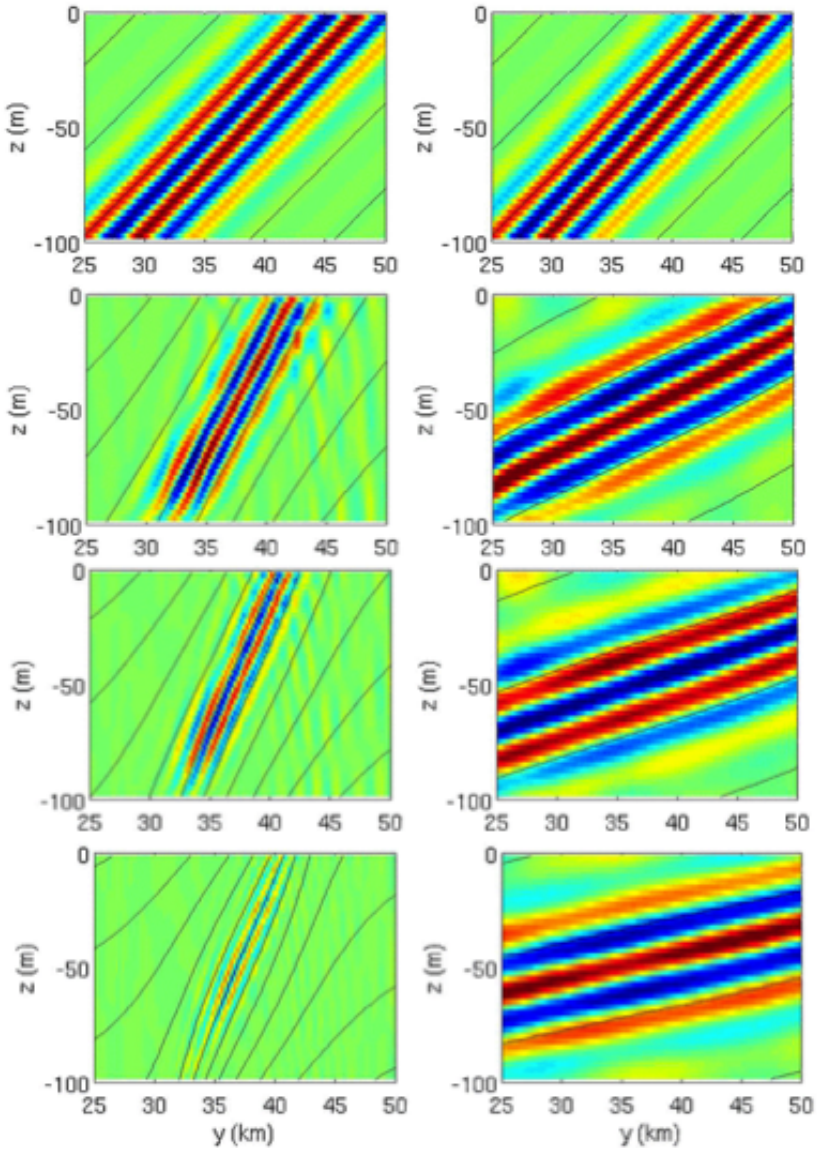

Fig. 14 Cross-sections of the y-component of the wave velocity field (color) and isopycnals (contours) at, from top to bottom, $t = 0, 2.9, 4.3$, and 5.7 inertial periods into the numerical simulation used to study NIWs in a front undergoing frontogenesis. The sections on the left (right) were made at $x = 18.75$ km ($x = 56.25$ km) in a region where the eddy-driven strain field is frontogenetic (frontolytic).

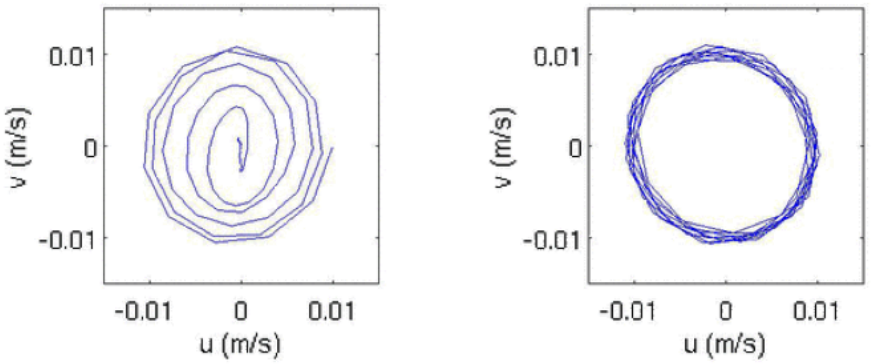

Fig. 15 Hodographs of the wave velocity at mid-depth ($z = -50$ m) and $y = 37.5$ km from the numerical simulation used to study NIWs in a front undergoing frontogenesis. The hodograph on the left (right) was made at $x = 18.75$ km ($x = 56.25$ km) in a region where the eddy-driven strain field is frontogenetic (frontolytic).

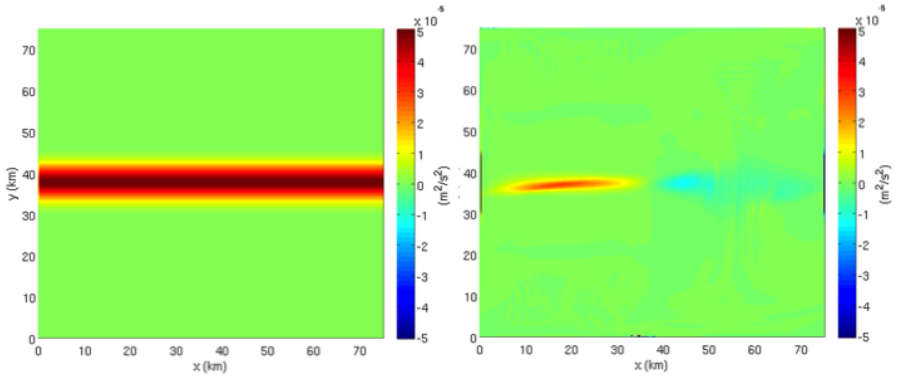

Fig. 16 Left: plan view of the KE in the NIW at the start of the numerical simulation used to study NIWs in a front undergoing frontogenesis. Right: plan view of the amount of KE removed from the strain field by the NIWs, i.e. $\int DSPdt$, eight inertial periods into the simulation. The colorbar is the same in both panels and both quantities are evaluated at mid-depth ($z = -50$ m).

profoundly alter the rules of wave reflection off surfaces. In particular, inertial waves with frequency f_{eff} experience critical reflection off the sea surface at fronts. Upon reflection, the vertical scale of the waves collapses, enhancing viscous dissipation. But through the process the waves dissipate more energy than that which they flux towards the surface. The extra energy comes from the front. Thus critical reflection at fronts is a mechanism dissipates energy in the NIW field and the balanced circulation simultaneously. It is therefore distinct from classical critical reflection of internal waves off bathymetry which only damps the waves. The rate at which energy is removed and dissipated from the front during critical reflection scales with the energy flux of the upward propagating inertial waves. Accounting for variations in the effective

Coriolis frequency, such waves could be generated remotely by the winds or tides, for example, and experience critical reflection if their frequency is equal to the local value of f_{eff} at the front. In this case, the dissipation of energy in the balanced circulation via critical reflection should scale with the rate of energy input into the waves by the winds or tides where they are generated.

Finally, the velocity hodographs of NIWs do not trace horizontal inertial circles at fronts. Instead, the wave velocity has a vertical component and is elliptically polarized with stronger flow in the cross-front direction. These modified polarization relations allow the waves to exchange kinetic energy with mean flows by driving wave momentum fluxes. The effects are enhanced with frontal intensity, and therefore are most pronounced in fronts undergoing frontogenesis. If the frontogenesis is driven by strain associated with mesoscale eddies, for example, the increasingly elliptically polarized wave velocities allow NIWs trapped in a front to efficiently extract KE from eddies. The energy is not stored in the wave field but is instead lost to cross-front ageostrophic motions. Hence, the NIWs act as a conduit that transfers KE from balanced eddies to unbalanced motions. As with critical reflection, the waves are ultimately damped in the process, therefore both mechanisms represent sinks of KE for the NIW wave field and mesoscale eddies. The rate and amount of KE removed from balanced motions by these processes could be significant since the theory suggests that it should scale with the NIW-generating energy fluxes and the KE contained in NIWs, respectively. Therefore quantifying the contributions of these processes to global energy budgets of the circulation and NIW field should be the focus of future work.

Acknowledgements This article reviews material that I was invited to present at the 48th Liege Colloquium on Submesoscale Processes: Mechanisms, Implications and New Frontiers. I would like to thank Alexander Barth, Eric Deleesnijder, Amala Mahadevan, Ananda Pascual, Simon Ruiz, and Charles Troupin for organizing such a stimulating meeting and inviting me to speak. This work was funded by the National Science Foundation grant OCE-1260312.

References

Alford M, Gregg M (2001) Near-inertial mixing: Modulation of shear,strain and microstructure at low latitude. J Geophys Res 106:16,947–16,968

Danioux E, Klein P, Rivière P (2008) Propagation of wind energy into the deep ocean through a fully turbulent mesoscale eddy field. J Phys Oceanogr 38:2224–2241

Danioux E, Vanneste J, Bühler O (2015) On the concentration of near-inertial waves in anticyclones. J Fluid Mech 773:R2

D'Asaro EA (1995) Upper-ocean inertial currents forced by a strong storm. PartIII: Interaction of inertial currents and mesoscale eddies. J Phys Oceanogr 25:2953–2958

Eliassen A (1962) On the vertical circulation in frontal zones. Geofys Publ 24:147–160

Elipot S, Lumpkin R, Prieto G (2010) Modification of inertial oscillations by the mesoscale eddy field. J Geophys Res 115:C09,010

Ferrari R, Wunsch C (2009) Ocean circulation kinetic energy: Reservoirs, sources, and sinks. Annu Rev Fluid Mech 41:253–282

Grisouard N, Thomas LN (2015) Critical and near-critical reflections of near-inertial waves off the sea surface at ocean fronts. J Fluid Mech 765:273–302

Grisouard N, Thomas LN (2016) Energy exchanges between density fronts and near-inertial waves reflecting off the ocean surface. J Phys Oceanogr 46:501–516
Ivey GN, Nokes RL (1989) Vertical mixing due to the breaking of critical internal waves on sloping boundaries. J Fluid Mech 204:479–500
Klein P, Hua BL, Carton X (2003) Emergence of cyclonic structures due to the interaction between near-inertial oscillations and mesoscale eddies. Qt J R Met Soc 129:2513–2525
Kunze E (1985) Near-inertial wave propagation in geostrophic shear. J Phys Oceanogr 15:544–565
Kunze E (1986) The mean and near-inertial velocity fields in a warm-core ring. J Phys Oceanogr 16:1444–1461
Kunze E, Sanford T (1984) Observations of near-inertial waves in a front. J Phys Oceanogr 14:566–581
Kunze E, Schmidt RW, Toole JM (1995) The energy balance in a warm-core ring's near-inertial critical layer. J Phys Oceanogr 25:942–957
Lee DK, Niiler PP (1998) The inertial chimney: The near-inertial energy drainage from the ocean surface to the deep layer. J Geophys Res 103:7579–7591
Mooers CNK (1975) Several effects of a baroclinic current on the cross-stream propagation of inertial-internal waves. Geophys Fluid Dyn 6:245–275
Müller P, Holloway G, Henyey F, Pomphrey N (1986) Nonlinear interactions among internal gravity waves. Rev Geophys 24:493–536
Plueddemann AJ, Farrar JT (2006) Observations and models of the energy flux from the wind to mixed-layer inertial currents. Deep-Sea Research II 53:5–30
Sawyer JS (1956) The vertical circulation at meterological fronts and its relation to frontogenesis. Proc Roy Soc London A234:346–362.
Thomas LN (2012) On the effects of frontogenetic strain on symmetric instability and inertia-gravity waves. J Fluid Mech pp 620–640
Thomas LN (2016) Near-inertial waves in fronts undergoing frontogenesis. J Phys Oceanogr In preparation
Thomas LN, Taylor JR (2014) Damping of inertial motions by parametric subharmonic instability in baroclinic currents. J Fluid Mech 743:280–294
van Meurs P (1998) Interactions between near-inertial mixed layer currents and the mesoscale: The importance of spatial variabilities in the vorticity field. J Phys Oceanogr 28:1363–1388
Whitt DB, Thomas LN (2013) Near-inertial waves in strongly baroclinic currents. J Phys Oceanogr 43:706–725
Xie JH, Vanneste J (2015) A generalised-Lagrangian-mean model of the interactions between near-inertial waves and mean flow. J Fluid Mech 774:143–169
Young WR, Ben-Jelloul M (1997) Propagation of near-inertial oscillations through a geostrophic flow. J Mar Res 55:735–766